water

MDPI

Article

The Use of TRMM 3B42 Product for Drought Monitoring in Mexico

Aurea De Jesús [1,2], Jose Agustín Breña-Naranjo [1,*], Adrián Pedrozo-Acuña [1] and Victor Hugo Alcocer Yamanaka [3]

1 Instituto de Ingeniería, Universidad Nacional Autónoma de México, Cd. Universitaria, 04510, CDMX, Mexico; adeJesusr@ii.unam.mx (A.D.J.); apedrozoa@ii.unam.mx (A.P.-A.)
2 Programa de Doctorado de la Facultad de Ingeniería Civil. Cd. Universitaria, 04510, CDMX, Mexico
3 Comisión Nacional del Agua, Insurgentes Sur 2416, 01020, CDMX, Mexico; yamanaka@conagua.gob.mx
* Correspondence: jbrenan@iingen.unam.mx; Tel.: +52-556-233-600 (ext. 8721)

Academic Editor: Athanasios Loukas
Received: 1 May 2016; Accepted: 27 July 2016; Published: 2 August 2016

Abstract: Drought has been a recurrent phenomenon in Mexico. For its assessment and monitoring, several studies have monitored meteorological droughts using standardized indices of precipitation deficits. Such conventional studies have mostly relied on rain gauge-based measurements, with the main limitation being the scarcity of rain gauge spatial coverage. This issue does not allow a robust spatial characterization of drought. A recent alternative for monitoring purposes can be found in satellite-based remote sensing of meteorological variables. The main objective of this study is to evaluate the standardized precipitation index (SPI) in Mexico during the period 1998 to 2013, using the Tropical Rainfall Measuring Mission (TRMM) satellite product 3B42. Results suggest that Mexico experienced the driest conditions during the great drought between 2011 and 2012; however, temporal variability in the SPI was found across different climatic regions. Nevertheless, a comparison of the SPI derived by TRMM against the rain gauge-based SPI computed by the official Mexican Drought Monitor showed low to medium correlation of the time series though both SPIs managed to capture the most relevant droughts at the national scale. We conclude that the TRMM product can properly monitor meteorological droughts despite its relative short dataset length (~15 years). Finally, we recommend an assimilation of rain gauge and satellite-based precipitation data to provide more robust estimates of meteorological drought severity.

Keywords: drought; SPI; rainfall; TRMM; Mexico

1. Introduction

Droughts are one of the most common natural hazards that can have impact on agricultural, ecological, social and economic consequences worldwide, and can often cause serious damage to crop production, limit water supply and even provoke human death. Drought is commonly defined as a period of deficit in precipitation or below normal water availability [1,2] and is characterized for being highly heterogeneous in space and variable in time [3].

Several indexes have been developed to help identify the onset and end of a drought as well as its severity for water and agricultural management purposes. Meteorological drought can be monitored using drought indices such as the Palmer Drought Severity Index (PDSI) [4], which is based on precipitation and air temperature deficits, or the Standardized Precipitation Index (SPI) developed by McKee et al. [5], which describes the cumulative probability of a rainfall occurrence over a given time period. Different studies have identified the usefulness of the SPI to quantify meteorological droughts [6–10]. In recent years, the National Drought Mitigation Center (NDMC) [11], the Western Regional Climate Center (WRCC) [12], the United States Department of Agriculture (USDA) [13] and

the Drought Monitor (USDM) [14,15], among others, have integrated this index for the assessment of drought intensity. Moreover, the SPI has been used for studying different aspects of droughts, such as its forecasting [16], frequency analysis [17], spatiotemporal analysis [18] and climate change impact studies [19].

The SPI only requires information about precipitation for its estimation, so it can characterize the amount of dryness or wetness over different time scales and is less complex to calculate than others meteorological indicators such as the PDSI. On the other hand, the SPI solely relies on atmospheric water supply and hence cannot account for other proxies of terrestrial dryness such as evapotranspiration, limiting to capture the effect of increased temperatures and fluctuations in the atmospheric water demand [20]. Although it is plausible to include additional variables to improve drought monitoring, the lack of long-term meteorological observations in several limited-data regions of the world makes the SPI the most used common drought index. However, in developing countries, ground-based rainfall observation networks are often sparsely distributed and can limit our understanding of climatological patterns [21].

In those regions with sparse weather stations, drought conditions may be estimated by means of spatial interpolation using geostatistical techniques. Although spatial interpolation helps to inferring drought conditions at large scales, it may have high uncertainties [22], which represents a substantial difficulty when dealing with effective spatial coverage of rainfall over a large area, mainly in mountainous regions. Alternatively, space borne remote sensing, which can be used to infer precipitation across the quasi-global scale can continuously monitor rainfall over large extensions and in near real-time [21]. Indeed, satellite information has become a feasible alternative to monitor droughts either by observing climatic conditions [22–24] or vegetation health [25], as input to operational hydrological models [26], for flood forecasting and early warning [27–30]. Satellite-based drought studies have assessed dryness conditions not only by monitoring precipitation, but also other key components of the water cycle such as soil moisture, snow, groundwater and evapotranspiration. For recent state-of-the-art remote sensing applications for drought monitoring and prediction, see [31].

Lack of knowledge of existing remote sensing products for drought monitoring has restrained the development and testing of observational tools for drought phenomena. Such is the case of Mexico, where the only drought monitoring tool relies on a very limited rain gauge network that spares regions with complex topography. Mexico's long-term precipitation regime is characterized by strong spatial precipitation gradients. While its northern portion that covers more than half of the country's area is well known for having persistent arid and semiarid climate conditions, the remaining southern portion ranges from a temperate regime located around the central regions to a humid tropical climate in the southernmost part, around the border with Guatemala. In spite of such great variability observed in the spatial distribution of precipitation, its temporal distribution is quite consistent across the country (an exception being the extreme northwestern region, close to California), which is characterized by relatively dry winters, whereas the rainfall season typically occurs from May–June until September–October.

Monitoring drought conditions in Mexico at the countrywide scale are recent. Since 1999, the North American Drought Monitor (NADM) has been the result of a technical cooperation among drought experts from Mexico, USA and Canada dedicated to describe dryness and wetness conditions in North America. However, it is until 2014 when an official Drought Monitor (MDM) was developed using in situ information to monitor meteorological drought conditions by means of the SPI. Although the MDM is computed following the North American Drought Monitor procedures (which is partially based on the US Drought Monitor, see [14]), the lack of ground information available in Mexico has reduced the number of variables involved in the computation of the drought index. Such index is a combination of meteorological drought (SPI, using the rain gauge network shown in Figure 1), agricultural drought (soil moisture deficits computed by a soil moisture leaky bucket model and the Normalized Difference Vegetation Index, NDVI) and hydrological drought (levels in reservoirs) [14,15].

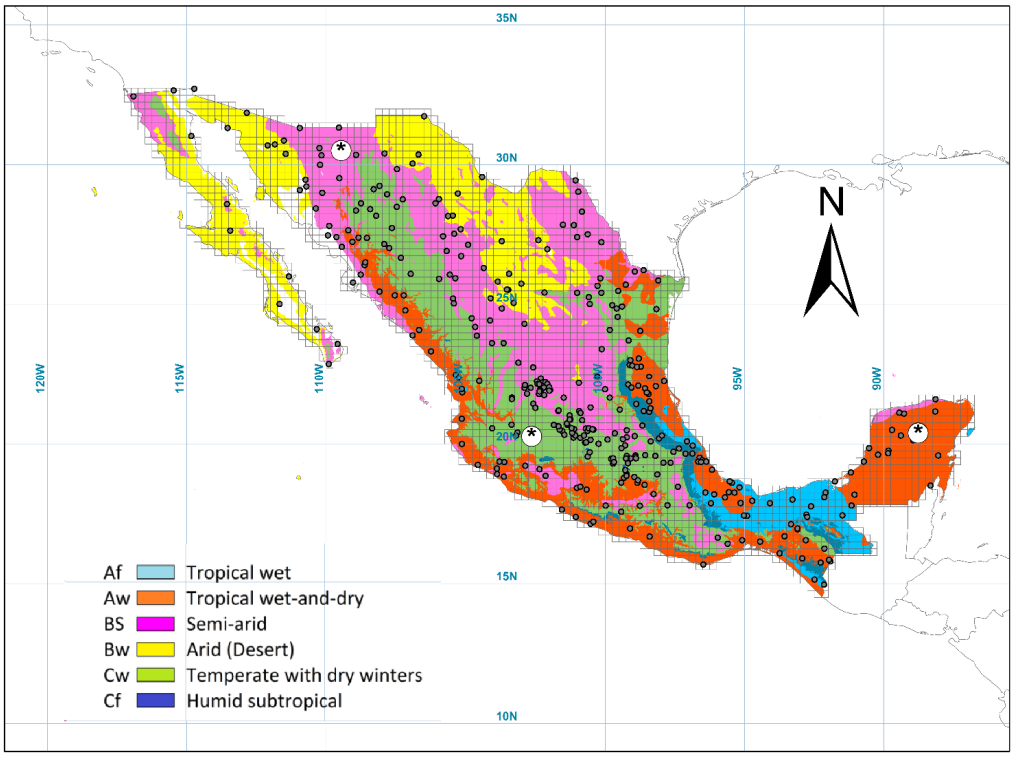

Figure 1. Climate classification of Mexico, location of the 364 rain gauges used to derive the drought index from the MDM and TRMM 3B42 spatial resolution grid (0.25° × 0.25°). Large circles with the asterisk represent those rain gauges whose SPI was compared against the SPI derived from the TRMM 3B42.

Previous research on droughts in Mexico has focused on different meteorological aspects such as the structure and variability of spatial modes [32], the potential use of tree-ring records from northern Mexico to indicate the historical drought occurrence from 1780 to 1992 [33,34], historical teleconnections between sea surface temperatures and El Niño Southern Oscillation induced droughts [35], classification of homogeneous climatic zones using the SPI [9] and drought vulnerability assessment [36]. Nevertheless, there are no drought monitoring studies in Mexico that use in situ measurements, data assimilation products or spaceborne datasets.

This work presents a satellite-based national-scale meteorological drought monitor for Mexico during the period 1998 to 2013. The monitor detects drought severity by means of the Standardized Precipitation Index (SPI) obtained from datasets derived by the spaceborne Tropical Multi-Precipitation Analysis (TMPA 3B42) product, which has the ability to quantify rainfall in tropical and temperate regions of the world. The specific goals of this study are to: (1) evaluate the SPI across Mexico's terrestrial surface over a 16 year period (1998–2014); (2) compare drought severity between this satellite-based SPI and the ground-based SPI from the MDM; and (3) analyze the drought patterns that occurred in Mexico during the 2011–2012 drought event.

2. Data and Methods

2.1. Site Description

Because the TRMM product almost covers the total global terrestrial and oceanic surface, the monitor was developed for the whole Mexican territory (Figure 1). Mexico is located in the geographical region delimited by 14°–33° N, 84°–118° W and is characterized by a wide range of climates and landscapes (Figure 1). Different climate regimes in Mexico are mainly controlled by the latitude and regional circulation systems that interact with the country's topography. According to

the Köppen climate classification system, Mexico can be divided into six different climate typologies: tropical wet zones (characterized by constant wetness throughout the year), tropical wet-and-dry zones (dry winters and wet summers), semiarid zones (250–750 mm of rain that mostly occurs during summer), arid zones (less than 250 mm of rain per year with dry and cold winters), temperate zones with dry winters (mild temperatures with annual rainfall ranging between 600 mm and 1200 mm) and humid tropical zones (mild temperatures with uniform rain patterns throughout the year) [37,38]. Semiarid and arid regions are mainly located in the northern half of the country, whereas the regions around the center of Mexico consist of temperate zones with dry winters. Finally, the south and coastal regions (with the exception of the north) have tropical wet or wet-and-dry regimes.

2.2. Data and Methodology

The precipitation dataset was extracted from the Tropical Multi-satellite Precipitation Analysis product TMPA 3B42 version 7 (hereafter TRMM 3B42). This product is a combination of different satellite remote sensors set up in the Tropical Rainfall Measuring Mission [39,40], namely Precipitation Radar (PR) and Microwave Imager (TMI) [41–43], both onboard TRMM satellite. In addition, the TMPA incorporates information from the Special Sensor Microwave Imager (SSM/I) onboard Defense Meteorological Satellite Program (DMSP) satellite [44,45], the Advanced Microwave Scanning Radiometer (AMSR) onboard US Earth Observing Satellite (EOS) "Aqua" [46,47] and the Advanced Microwave Sounding Unit (AMSU) onboard NOAA and MetOP satellites [48,49]. The TRMM 3B42 product consists of a 0.25×0.25 grid providing daily and three-hourly estimates that were calibrated with the support of observed monthly precipitation rates [39]. The main difference between TRMM 3B42 and TRMM 3B42 RT is that the latter product is computed in near-real time without any calibration and rain gauge-based corrections unlike the former. In this work, daily TRMM data covering Mexico's terrestrial surface were aggregated to obtain monthly estimates of precipitation across a grid covering 3020 TRMM 3B42 cells. Monthly time series (January 1998 to December 2013) for each cell were analyzed in order to derive the SPI for durations corresponding to one, three, six and twelve months, respectively.

The Standardized Precipitation Index (SPI) [5] was intended to be a spatially invariant indicator of drought, as it is based on long-term precipitation records [50,51]. The SPI is a quantitative indicator for negative and positive rainfall anomalies over different timescales so it can be used as a cumulative proxy for dry and wet conditions. The SPI calculation is based on the goodness-of-fit of the observed precipitation to a probability distribution such as the Pearson Type III [52] or Gamma probability density function [53].

As a result, positive SPI values indicate greater than median precipitation, and negative values indicate less than median precipitation. SPI values of less than -1 indicate that a drought event is taking place and its intensity can be calculated by accumulating the SPI values for any desired period (1, 3, 6, 9, 12, and 24 months, and so on). However, it is important to point out that for dry climates (such as the center and north of Mexico), short-term SPIs can hardly reveal any drought patterns as dry conditions can be dominant during several months of every year. Dryness and wetness severity can be classified into seven categories as suggested by McKee [5,6]: extremely dry (<-2), severely dry (-2 to -1.5), moderately dry (-1.5 to -1), near normal (-1 to 1), moderately wet (1 to 1.5), very wet (1.5 to 2) and extremely wet (>2).

3. Results and Discussion

The rainfall climatology observed in Mexico for the period 1998–2013 according to the TRMM 3B42 dataset is shown in Figure 2 and its average intra-annual variability is displayed in the inset. The annual map shows an overall dry precipitation regime (200 ± 100 mm/year) in the northern part of the country, whereas the southeastern part receives precipitation on average an order of magnitude higher (2000 ± 500 mm/year). Increasing gradients of precipitation can be observed from the Mexican High Plateau towards the western and eastern Sierra Madre mountains range. With the exception of

the northwestern portion (Lower California peninsula and Sonora's coast), Mexico's coastal regions receive on average more than 1000 mm of rain per year. The region with the greatest precipitation gradients and higher values are located along the narrowest continental strip in southern Mexico, most specifically in the upper areas of Oaxaca and Chiapas and the floodplains of Veracruz and Tabasco. As shown in the sub-window, on average, Mexico's precipitation regime is highly seasonal, with only 14.4% of the annual rainfall occurring between December and April and the rest (~85.6%) from May until November.

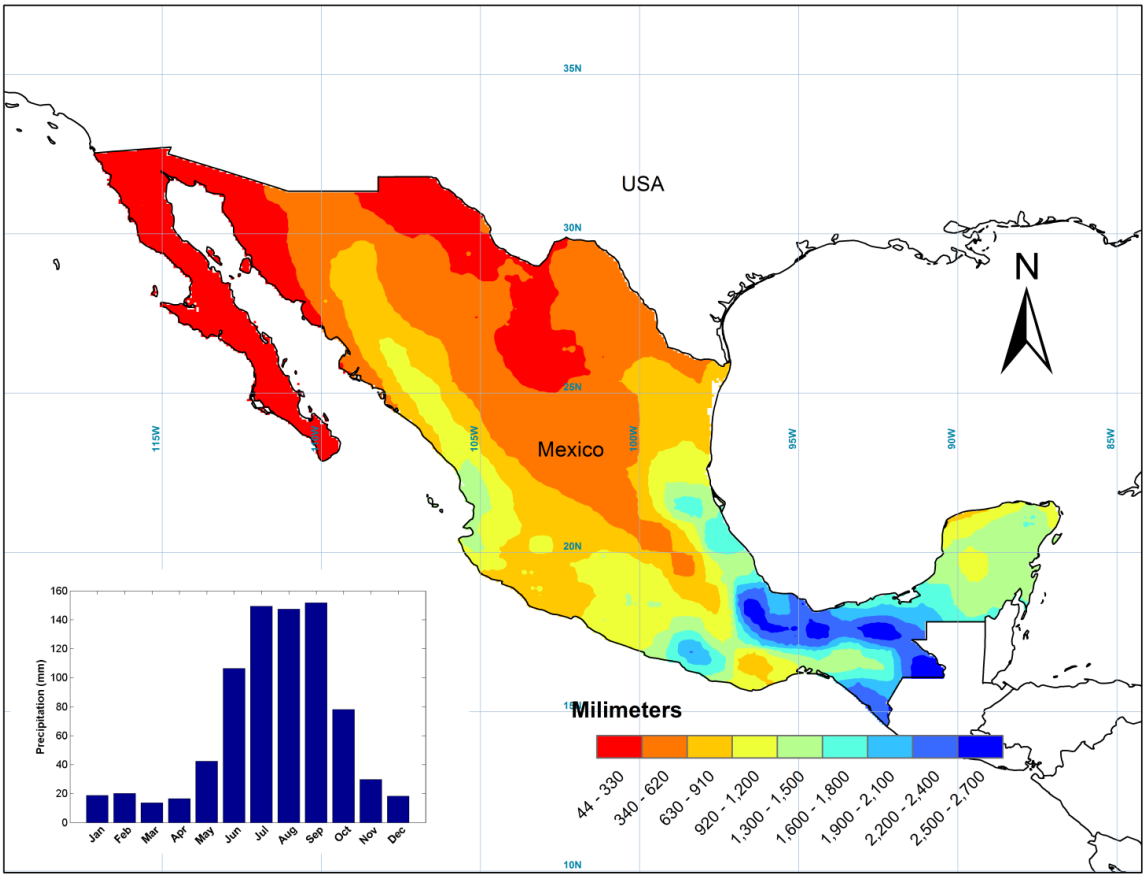

Figure 2. TRMM 3B42 derived map of mean annual precipitation in Mexico between 1998 and 2013. The inset displays the monthly precipitation climatology averaged over Mexico.

In addition to the spaceborne-based Mexico's rainfall climatology shown in the previous figure, rainfall anomalies (the difference between monthly precipitation records and its long-term average) were calculated so that a more clear distinction between dry and wet climatological monthly conditions can be inferred (see Figure 3). In this figure, monthly anomalies of precipitation range between −50 and +50 mm with an exception in July of 2010, which exceeds 80 mm. In contrast, there is a deficit close to 50 mm in 2000, 2009, 2010 and 2011, with an exception observed in October 2010 and September 2011, where minima values for the 15-year period of analysis were reached. In spite of such observed continuous deficit in precipitation in 2011, the positive one-month anomaly during summer seems to have provided some relief to drought conditions.

The temporal evolution of nationwide SPIs is shown in Figure 4. Grey lines indicate the standardized values of individual TRMM cells located in Mexico and the filled areas (blue and red) represent the average monthly SPI. The average over the whole country time series of SPI-1 (Figure 4a) illustrates very well precipitation seasonality. A similar seasonal pattern is observed, displayed with smoother contours, in the average time series for SPI-3 (Figure 4b) and SPI-6 (Figure 4c). Although SPI values for short timescales accurately describe the cyclical behavior of the precipitation regime, they

fail to indicate clearly a drought occurrence. However, as the timescale reaches cumulative durations of at least 12 months (Figure 4d), the separation between persistent dry and wet periods becomes more evident and can reflect the potential impacts of long periods of dryness on agriculture and water supply.

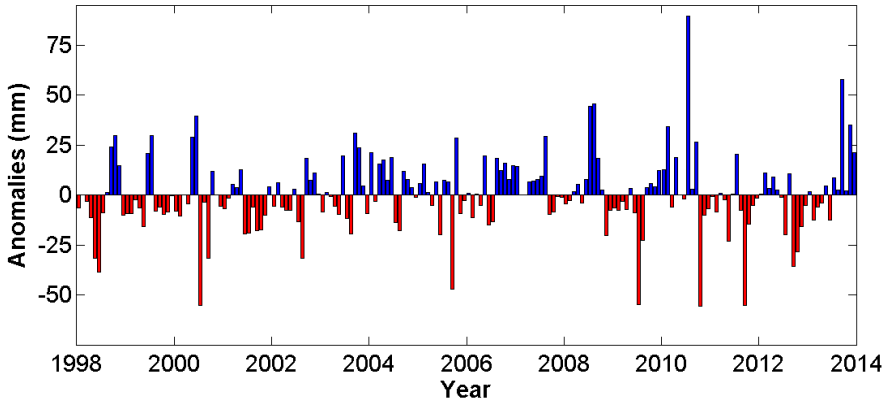

Figure 3. Spatially averaged monthly anomalies of precipitation in Mexico (1998–2013) derived from the TRMM 3B42 product.

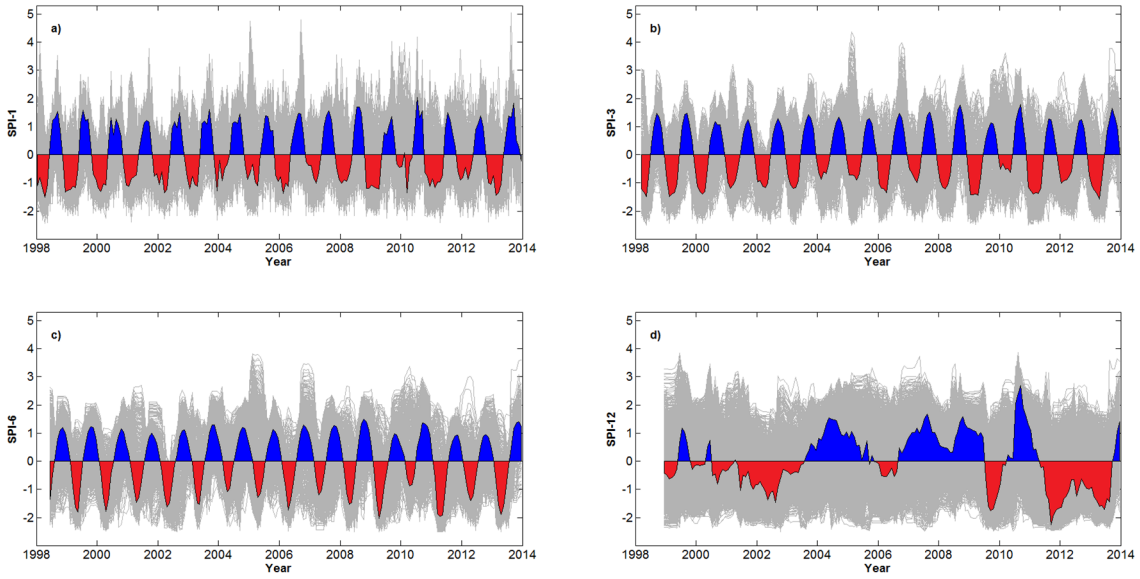

Figure 4. Standardized Precipitation Index (SPI) averaged over Mexico from 1998 until 2014 at different timescales: one month (**a**); three months (**b**); six months (**c**); and twelve months (**d**).

According to the SPI-12, drought events were clearly detected in 2000–2003, 2006, 2009 and 2011–2013, with normal and/or wet periods between them. It is important to stress that these SPI values represent average conditions over Mexico, so more severe wet or dry conditions at the local or regional scales might have occurred but are difficult to observe when the time series are spatially aggregated to the national scale.

A more detailed perspective on drought conditions across several climatic zones of Mexico is displayed in Figure 5 and shows some significant temporal variability in drought occurrence across the different study sites. For instance, when the SPI-12 chart (Figure 5d) is examined, it reveals that some climatic zones experienced their worst drought conditions before the great drought of 2011–2012 such as the Aw (tropical wet-and-dry regions, in 2009), Bw (arid regions, in 2002) and Cf (humid

subtropical, in 2009), whereas other regions dealt with important dry conditions after the great drought such as Af (tropical wet, in 2013). The remaining regions, BS (semi-arid) and Cw (temperate with dry winters), were the most severely affected during the great drought. It is important to note that drought conditions using shorter timescales than 12 months (1, 3 and 6 months) do not show marked differences among the climatic regions.

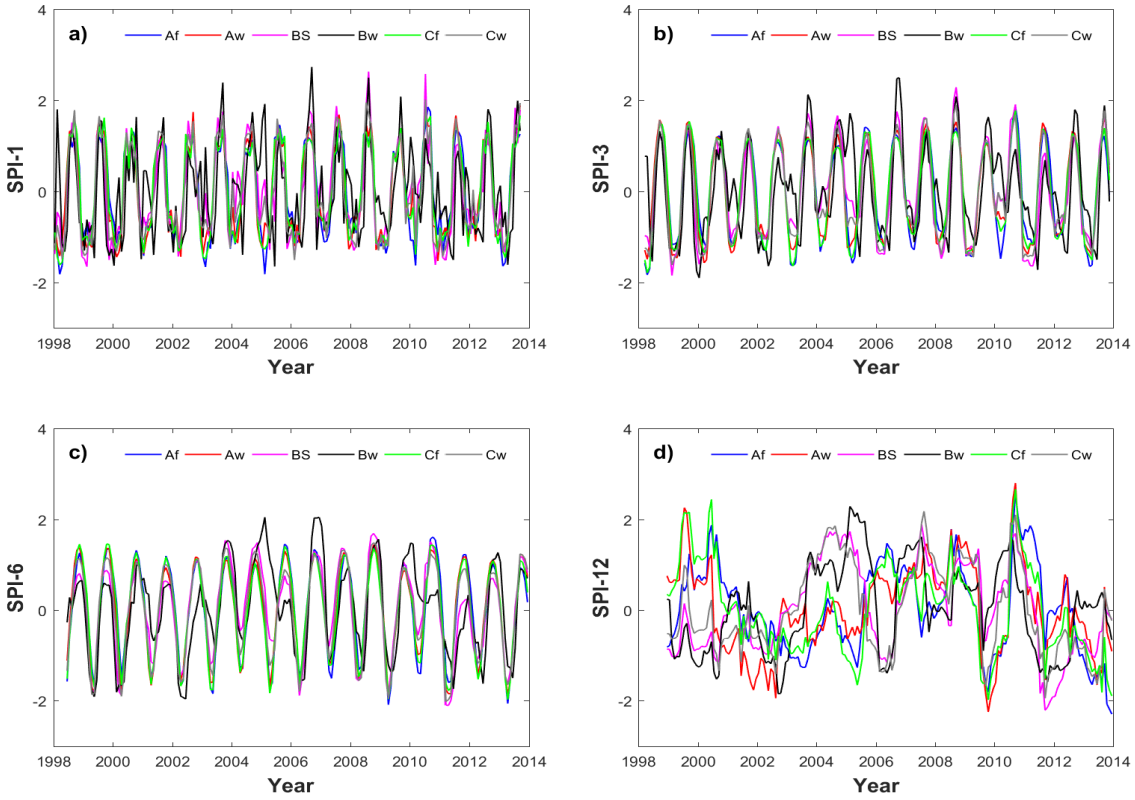

Figure 5. Standardized Precipitation Index (SPI) averaged over Mexico from 1998 until 2014 at different climate regions (color lines) and timescales: one month (**a**); three months (**b**); six months (**c**); and twelve months (**d**).

Even though this work tests the capability in monitoring climatological drought conditions with satellite-based precipitation, comparing both datasets can provide new insights about the probability of detection, false alarms and other potential errors in drought monitoring. Figures 6–8 suggest that the correlation between the SPI time series (rain gauges and satellite) is predominantly low (r values between 0.01 and 0.79), however these results show that the agreement in both SPIs to mimic the exceptional drought of 2011–2012 at local scales is in general quite high despite some gaps in the rain gauge time series (e.g., SPI-6 and -12 in Figures 6 and 7) or observed inconsistencies (e.g., early 2002 in Figure 7). In this context, although it is plausible to perform a more robust quantitatively analysis between both SPIs (e.g., incorporate more statistical indexes, and perform multi-category analysis), substantial differences in the time series length (records in several of the SPI rain gauges date back from the 1950s) and in the measured monthly precipitation are both potential sources of bias and therefore not very suitable for direct comparisons.

Low statistical correlation between the time series clearly suggests that the temporal fluctuations in the SPI do not follow the same pattern. This behavior can be attributed to the statistical parameters of both indices that are sensitive to the following factors: the length of the precipitation records from which the SPI was computed [51] and poor agreement in rainfall quantitative estimates due to scaling issues between the typical spatial footprint of a rain gauge and a mesoscale gridded product. A recent TRMM 3B42 validation study carried out in southern Mexico found that monthly precipitation

observed by TRMM during the dry season typically exceeds estimates from rain gauges whereas the opposite behavior occurs during the rainfall season (unpublished work).

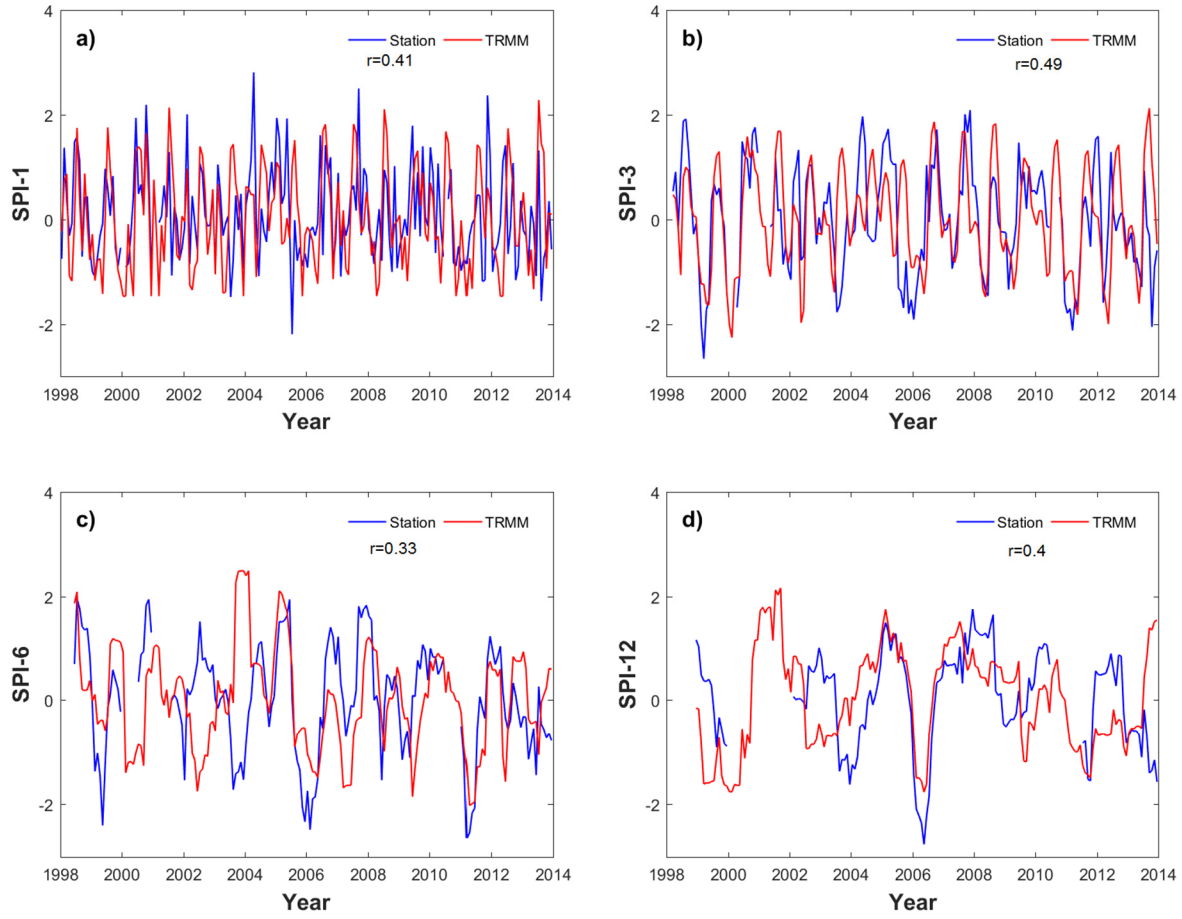

Figure 6. Comparison of SPI time series (TRMM-derived, blue line; Rain gauge derived, red line) at an arid climate (Sonora state in the north of Mexico) for different timescales: one month (**a**); three months (**b**); six months (**c**); and twelve months (**d**). Pearson's r correlation coefficient depicts the statistical agreement between both datasets.

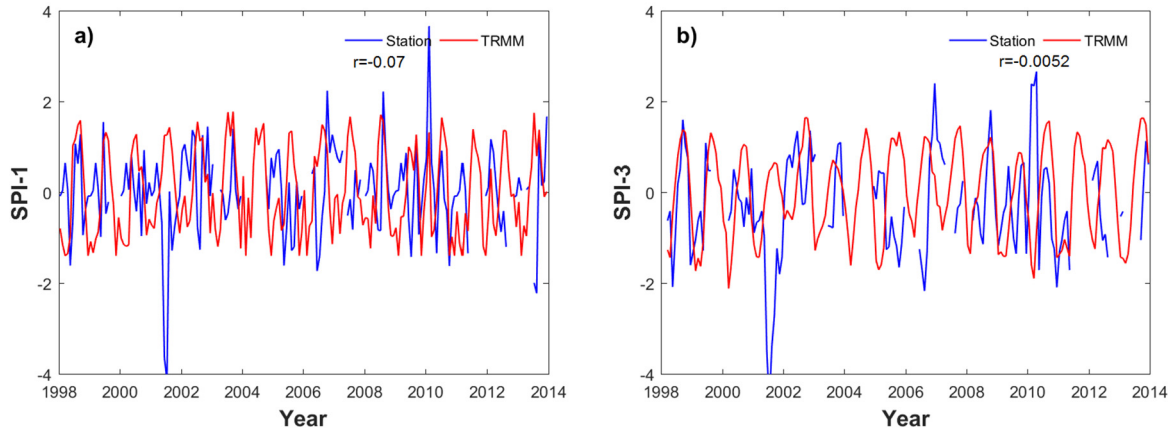

Figure 7. *Cont.*

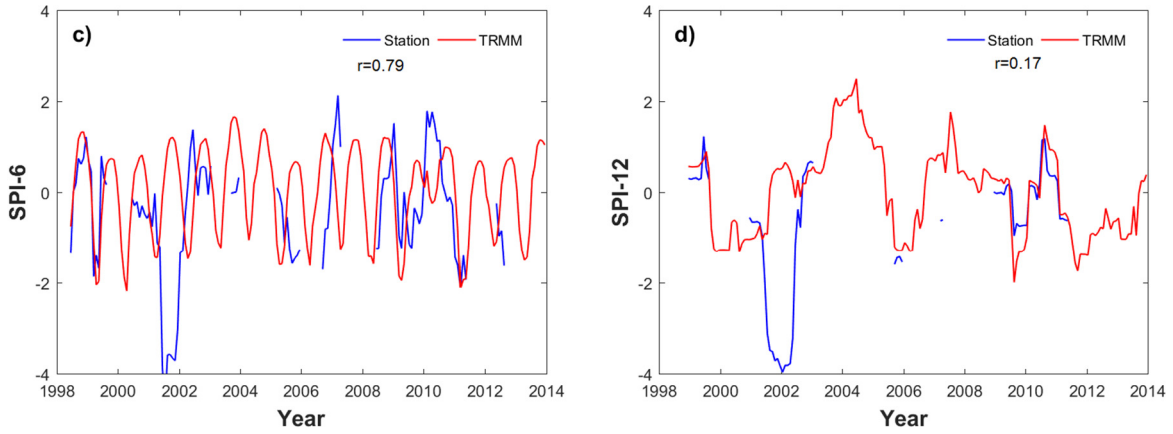

Figure 7. Comparison of SPI time series (TRMM-derived, blue line; Rain gauge derived, red line) at a temperate climate (Michoacán state in the central part of Mexico) for different timescales: one month (**a**); three months (**b**); six months (**c**); and twelve months (**d**). Pearson's r correlation coefficient depicts the statistical agreement between both datasets.

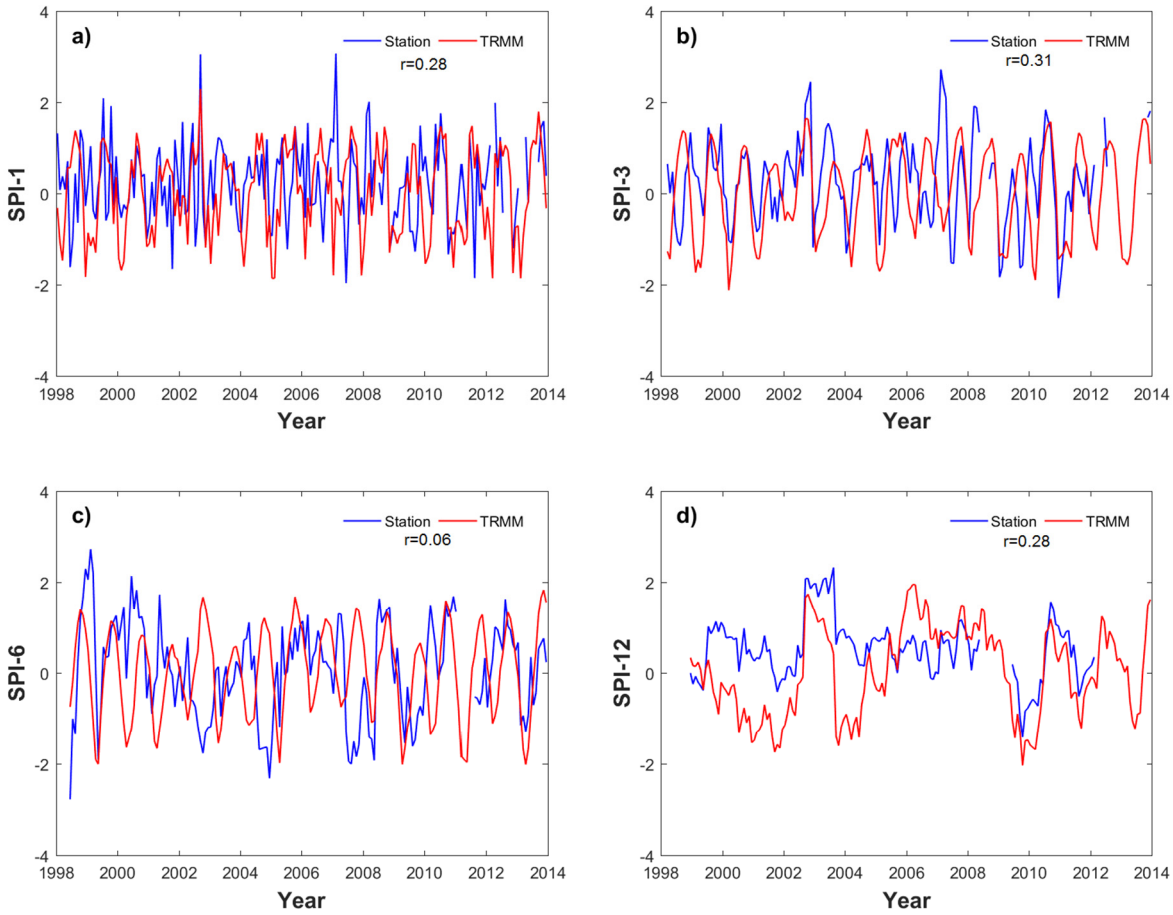

Figure 8. Comparison of SPI time series (TRMM-derived, blue line; Rain gauge derived, red line) at a humid climate (Yucatán state in the southeast of Mexico) for different timescales: one month (**a**); three months (**b**); six months (**c**); and twelve months (**d**). Pearson's r correlation coefficient depicts the statistical agreement between both datasets.

Spatially distributed SPI time series can also be used to assess the fraction or percentage of land under drought conditions as displayed in Figure 9. The graph shows the temporal variability of

Mexico's total surface affected by moderately dry (areas in dark yellow), severely dry (areas in red) and extremely dry (areas in dark red) conditions for different timescales (SPI-1, -3, -6 and -12). According to short-term SPIs (1, 3 and 6 months), the most severe year in terms of drought severity was 2011, whereas the long-term SPI (12 months) suggests a slow but substantial increase in the affected area by drought that covered up to two thirds of the country from 2011 until 2013.

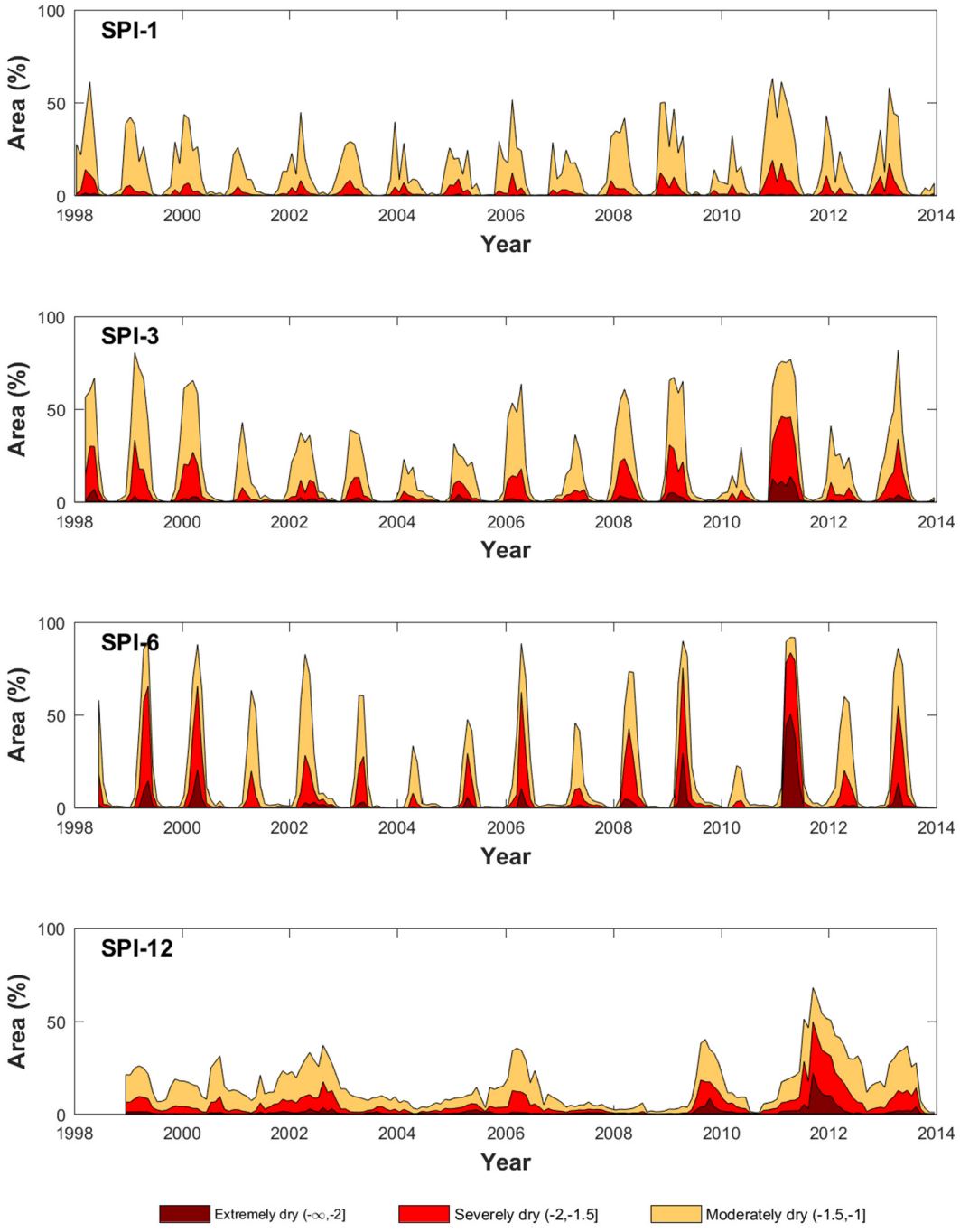

Figure 9. TRMM 3B42-based temporal evolution (1998–2013) of Mexico's terrestrial surface affected by drought conditions (moderate, severe and extreme) and for different SPI timescales (one, three, six and twelve months).

Due to the relevance of the 2011 drought, its spatial behavior (SPI of 3, 6 and 12 months, respectively) during and after its peak through the SPI maps is displayed in Figures 10–15.

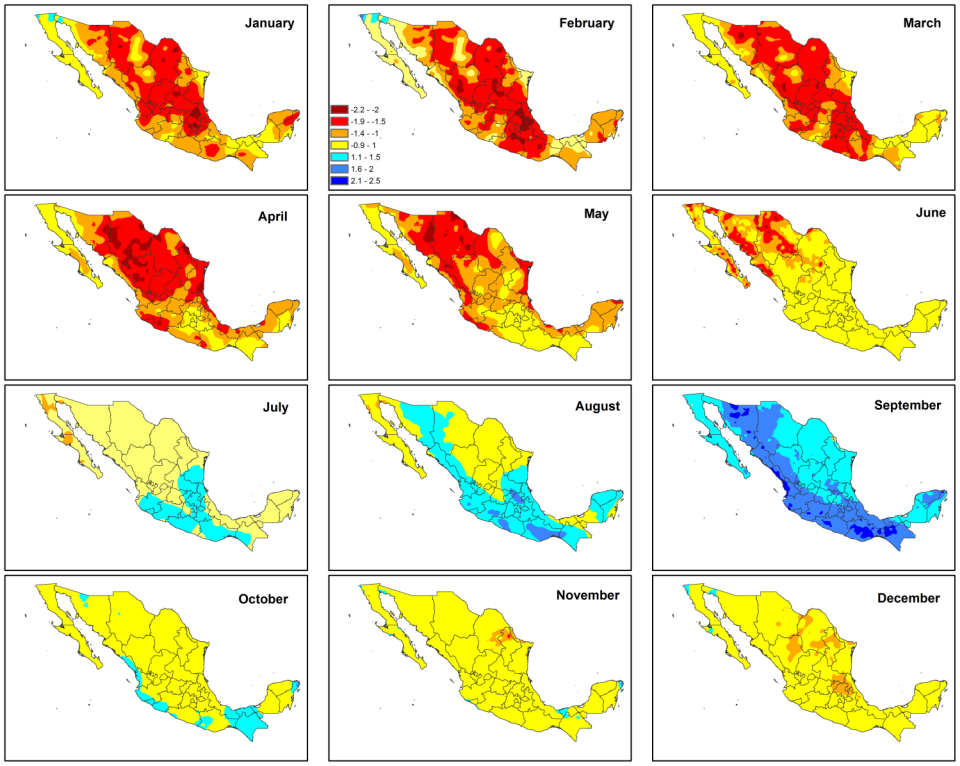

Figure 10. Drought monitoring based on TRMM 3B42 three-month Standardized Precipitation Index for 2011.

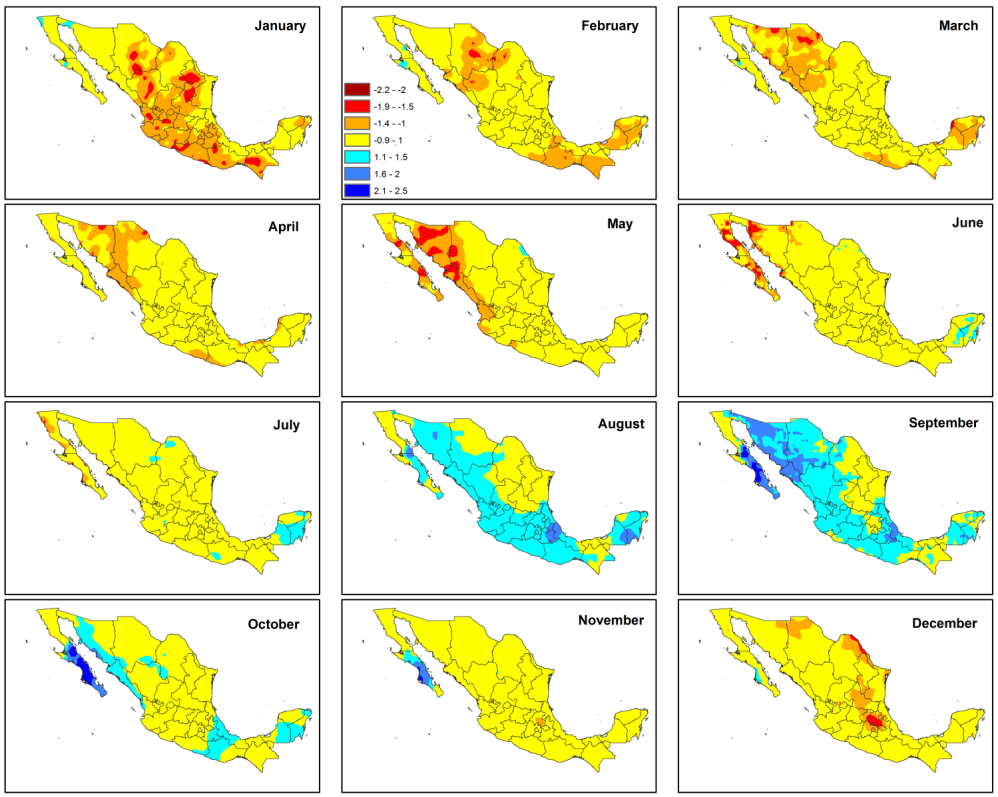

Figure 11. Drought monitoring based on TRMM 3B42 three-month Standardized Precipitation Index for 2012.

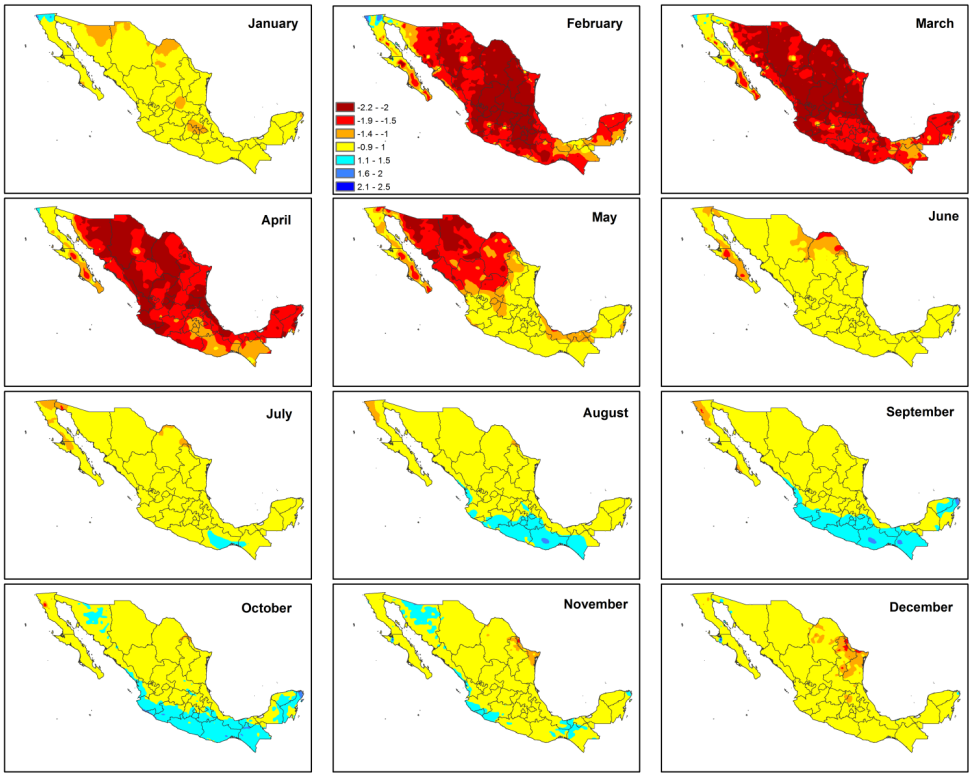

Figure 12. Drought monitoring based on TRMM 3B42 six-month Standardized Precipitation Index for 2011.

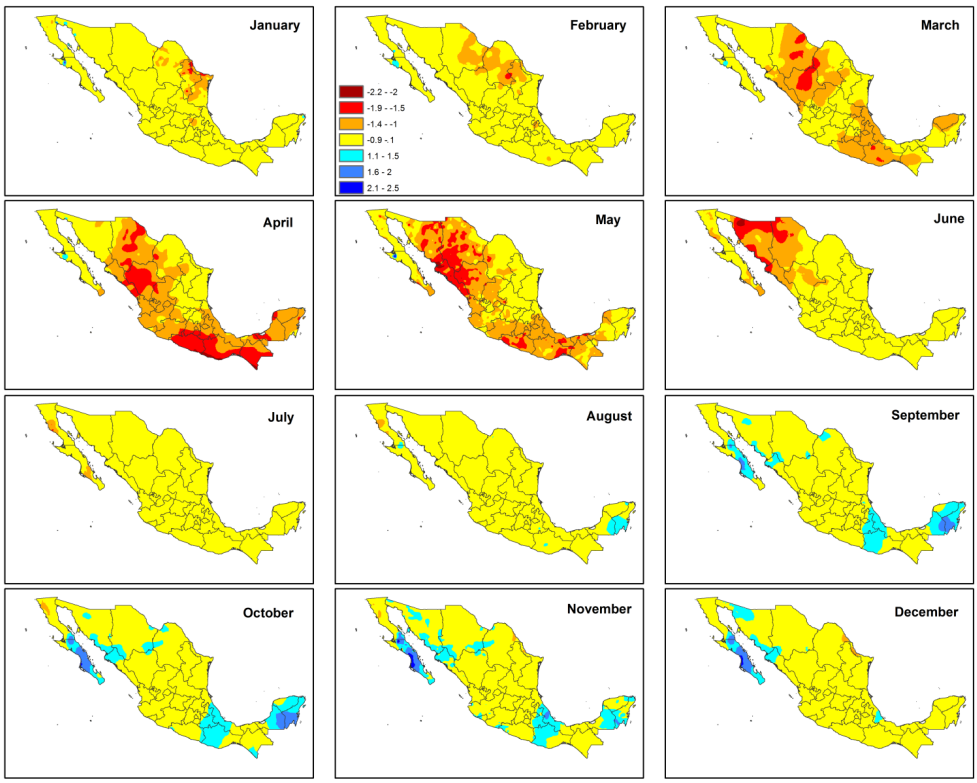

Figure 13. Drought monitoring based on TRMM 3B42 six-month Standardized Precipitation Index for 2012.

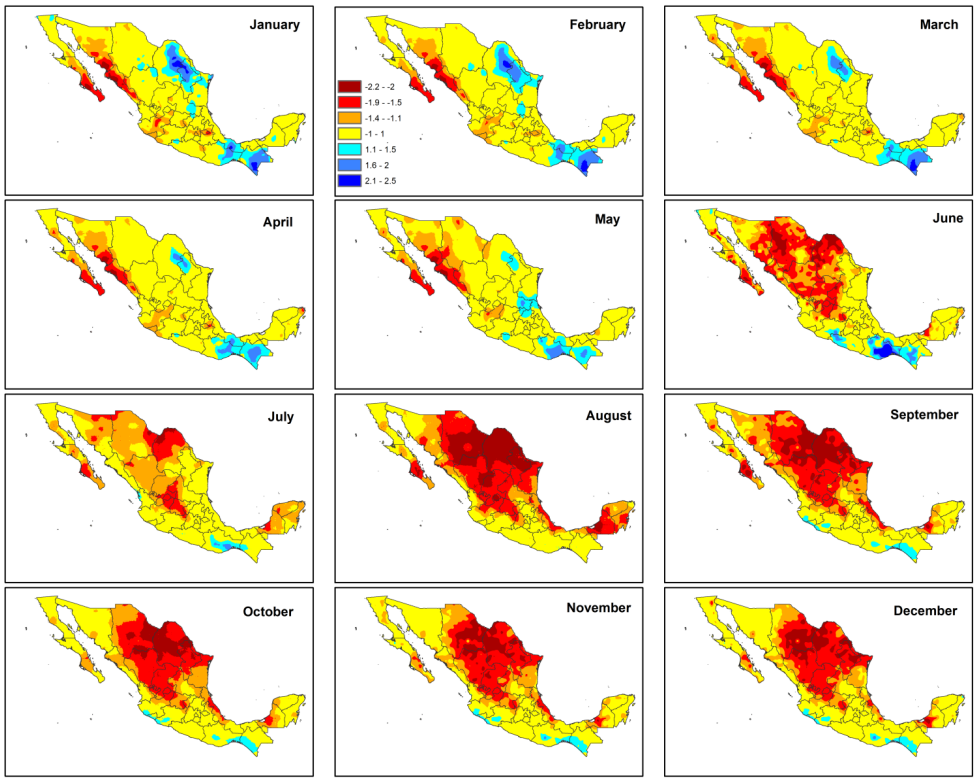

Figure 14. Drought monitoring based on TRMM 3B42 twelve-month Standardized Precipitation Index for 2011.

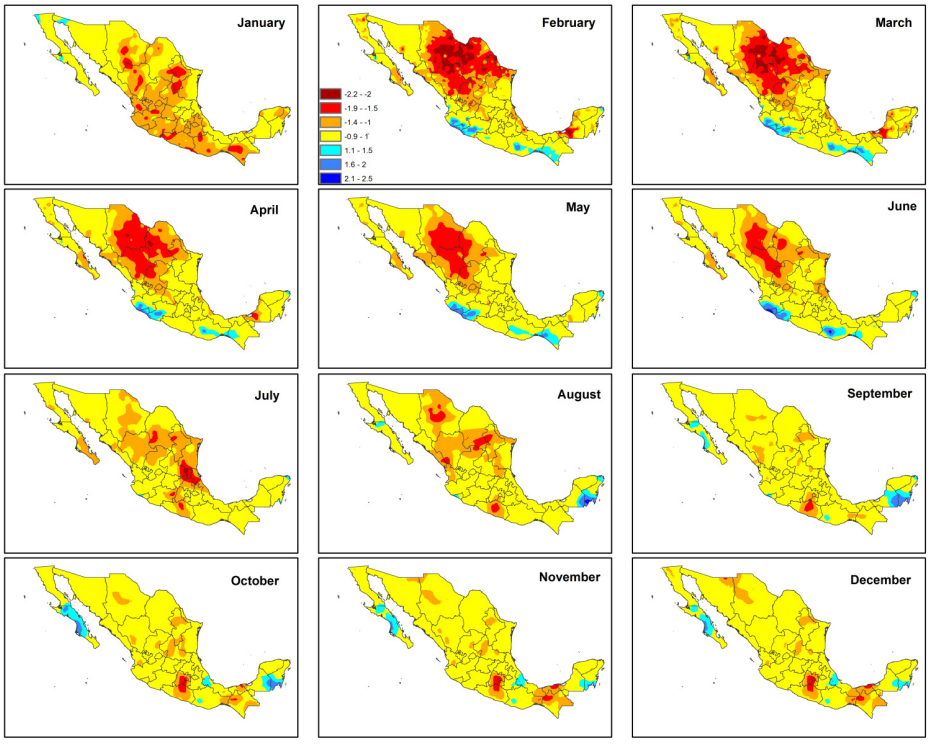

Figure 15. Drought monitoring based on TRMM 3B42 twelve-month Standardized Precipitation Index for 2012.

As illustrated in Figure 10, drought patterns for the SPI-3 during 2011 indicate that, in the first five months of the year, most of the country experienced very dry to extreme dry conditions followed by a two-month transitional period that interrupted the drought severity observed in the earlier months. Although September was the only month of the year with dominant humid conditions, the summer and fall seasons did not show any sign of wetness even though these seasons are typically characterized for being the wettest period of the year.

A comparison between the SPI-3 from 2011 and that from 2012 is shown in Figure 11. Overall, drought severity and its impacted areas during the first six months of 2012 were less intense compared to the same period during 2011. The months of January and May showed the driest conditions during 2012 though they were more moderate than those observed a year earlier and surprisingly the months between January and May did not show any clear drying patterns. The beginning of the rainy season in June did not lead to an abrupt end in drought as countrywide wetness was only observed in August and September.

According to the SPI-6 during 2011 (Figure 12), drought conditions followed a similar pattern than those observed by the SPI-3, but its severity was more visible between February and May. This suggests that the meteorological drought of 2011 was more sensitive to rainfall deficits at this scale. On the other side, the foremost rainy season of the year (July, August, and September) was also dryer for the SPI-6 compared to the SPI-3.

In Figure 13, it can be observed that drought transitioned from moderate severity in January–February to extreme severity in March–June, with the most affected areas mainly located in the western parts of the country. Drought conditions attenuated since July until the end of the year.

As shown in Figure 14, the most severe dry conditions for the SPI-12 in 2011 were detected during the second half of the year. The first half of the year indicates substantial spatial heterogeneity of the SPI across Mexico where the northwest region had persistent negative values, whereas the northeast and southeast regions experienced positive anomalies of precipitation. However, because of the lag time in this cumulative twelve-month period, dryness conditions can be traced back to the late 2010 and early 2011.

The SPI-12 in 2012 (Figure 15) reflected long-term precipitation patterns for the previously explained reason. Thus, moderate and severe droughts in April, May and June, in the north and center of the country were linked to dryness conditions experienced a year earlier. In the months of July and August, drought severity decreased across the north while, in the remaining months, there was severe drought across a few hotspots located in the south of Mexico.

4. Conclusions

Thus far, there has been a lack of scientific studies aimdd at assessing the severity, propagation and socio-economic impacts of contemporary droughts in Mexico. This work focuses in the first topic: monitoring drought conditions using a spaceborne gridded product with continuous daily information since the beginning of the 21st century (1998–2013). This period was characterized for having the most important drought in Mexico in terms of agricultural losses observed since the beginning of the 20th century [37,38,54,55]. In this paper, the Standardized Precipitation Index (SPI) was used to evaluate the drought conditions based on a monthly precipitation dataset (TRMM 3B42). Results were compared against drought severity estimates from a rain gauge network composed of ~350 stations. Although the rain gauge-based SPI is based on long-term statistics, several issues arise, such as the reliability and uncertainty that exist because of large spatial data gaps (the network of rain gauge stations is not representative of the whole country as there are significant gaps in several regions, personal communication from the National Weather Service staff) and larger spatial footprints by the TRMM product. On the other side, the satellite-based SPI can be useful for monitoring drought with a homogeneous resolution dataset, despite a shorter observational record that ultimately affect the statistical extreme distribution of precipitation.

Large scale seasonal patterns of drought were observed in the countrywide maps showing the three- and six-month SPI. However, the persistency was more evident using the SPI-12, because this timescale represents the cumulative result of shorter periods characterized for having statistically precipitation deficits. However, when SPI time series were analyzed by climatic regions (instead of its countrywide average), the most intense droughts in each region showed different timing under the SPI-12, with only two out of six regions reaching minima SPI values during the great 2011–2012 drought, whereas the remaining four regions experienced severe-to-extreme dryness at other times between 1998 and 2013. This suggests that the SPI-12 is the most appropriate scale to characterize meteorological droughts in Mexico as it allows differentiating drought patterns at the regional/local scale by showing evidence that droughts are not homogeneous in space and time (and hence its impact on the agricultural and hydrological component can also differ). Nevertheless, the largest percentage of area affected by drought was found by the SPI-6, especially for those regions with drought conditions classified as severely dry and extremely dry.

This work showed the potential of using a spaceborne precipitation product for monitoring meteorological drought. Results showed that the SPI derived either from rain gauges or from the TRMM 3B42 product can detect severe drought episodes, such as the great drought of 2011–2012. Future work should continue to validate and improve drought monitoring by merging satellite precipitation products with in situ precipitation data and by linking drought severity by means of remote sensing products to observed impacts on human activities such as agriculture and water supply.

Acknowledgments: The first author was supported by the CONACYT postgraduate scholarship program. The second author acknowledges financial support from UNAM's Institute of Engineering internal grant IING/DIR/044/2016.

Author Contributions: Jose Agustín Breña-Naranjo & Adrián Pedrozo-Acuña conceived and designed the design of the study; Aurea De Jesus performed the data analysis; Jose Agustín Breña-Naranjo, Adrián Pedrozo-Acuña & Victor Hugo Alcocer Yamanaka discussed and interpreted the results; Aurea De Jesus, Adrián Pedrozo-Acuña, Jose Agustín Breña-Naranjo & Victor Hugo Alcocer Yamanaka wrote the paper.

Conflicts of Interest: The authors declare no conflict of interest.

References

1. Du, L.; Tian, Q.; Yu, T.; Meng, Q.; Jancso, T.; Udvardy, P.; Huang, Y. A comprehensive drought monitoring method integrating MODIS and TRMM data. *Int. J. Appl. Earth Obs. Geoinform.* **2013**, *23*, 245–253. [CrossRef]
2. Van Loon, A.F.; Laaha, G. Hydrological drought severity explained by climate and catchment characteristics. *J. Hydrol.* **2014**, *526*, 3–14. [CrossRef]
3. Vicente-Serrano, S.M.; Beguería, S.; Lorenzo-Lacruz, J.; Camarero, J.J.; López-Moreno, J.I.; Azorin-Molina, C.; Revuelto, J.; Morán-Tejeda, E.; Sanchez-Lorenzo, A. Performance of drought índices for ecological, agricultural and hydrological applications. *Earth Interact.* **2012**, *16*, 1–27. [CrossRef]
4. Palmer, W.C. *Meteorological Drought*; Research Paper No. 45; U.S. Weather Bureau: Washington, DC, USA, 1965; pp. 9–18.
5. McKee, T.B.; Doesken, N.J.; Kleist, J. The relationship of drought frequency and duration to time scales. In Proceedings of the 8th Conference on Applied Climatology, Anaheim, CA, USA, 17–22 January 1993; American Meteorological Society: Boston, MA, USA, 1993; pp. 179–184.
6. McKee, T.B.; Doesken, N.J.; Kleist, J. Drought monitoring with multiple time scales. In Proceedings of the 9th Conference on Applied Climatology, Dallas, TX, USA, 15–20 January 1995; American Meteorological Society: Boston, MA, USA, 1995; pp. 233–236.
7. Shahid, S.; Marvili, M.D.; Farsani, P.A. Zoning Droughts by Standardized Precipitation Index in Esfahan Province (Iran). *IJABBR* **2013**, *1*, 477–481.
8. Vicente-Serrano, S.M.; Lopez-Moreno, J.I. Hydrological response to different time scales of climatological drought: An evaluation of the standardized precipitation index in a mountainous Mediterranean basin. *Hydrol. Earth Syst. Sci.* **2005**, *9*, 523–533. [CrossRef]
9. Giddings, L.; Soto, M.; Rutherford, B.M.; Maarouf, A. Standardized precipitation index zones for Mexico. *Atmosphera* **2005**, *18*, 33–56.

10. Hayes, M.J.; Svoboda, M.D.; Wilhite, D.A.; Vanyarkho, O.V. Monitoring the 1996 drought using the Standardized Precipitation Index. *Bull. Am. Meteorol. Soc.* **1999**, *80*, 429–438. [CrossRef]
11. National Drought Mitigation Center (NDMC) Homepage. Available online: http://drought.unl.edu (accessed on 14 December 2015).
12. Western Regional Climate Center (WRCC). Standardized Precipitation Index. 2000. Available online: http://www.wrcc.dri.edu/spi.html (accessed on 14 December 2015).
13. United States Department of Agriculture (USDA). Available online: http://www.usda.gov/nass/ (accessed on 14 December 2015).
14. Svoboda, M.; LeComte, D.; Hayes, M.; Heim, R.; Gleason, K.; Angel, J.; Rippey, B.; Tinker, R.; Palecki, M.; Stooksbury, D.; et al. The drought monitor. *Bull. Am. Meteorol. Soc.* **2002**, *83*, 1181–1190.
15. Heim, R.R., Jr. A Review of Twentieth-Century Drought Indices Used in the United States. *Bull. Am. Meteorol. Soc.* **2002**, *83*, 1149–1165.
16. Cancelliere, A.; Di Mauro, G.; Bonaccorso, B.; Rossi, G. Drought forecasting using the Standardized Precipitation Index. *Water Resour. Manag.* **2007**, *21*, 801–819. [CrossRef]
17. Thomas, T.; Nayak, P.; Ghosh, N. Spatiotemporal Analysis of Drought Characteristics in the Bundelkhand Region of Central India using the Standardized Precipitation Index. *J. Hydrol. Eng.* **2015**, *20*, 05015004. [CrossRef]
18. Almedeij, J. Drought Analysis for Kuwait Using Standardized Precipitation Index. *Sci. World J.* **2014**, *2014*, 451841. [CrossRef] [PubMed]
19. Lloyd-Hughes, B.; Saunders, M. A drought climatology for Europe. *Int. J. Climatol.* **2002**, *22*, 1571–1592. [CrossRef]
20. Vicente-Serrano, S.M.; Santiago, B.; López-Moreno, J.I. A Multi-scalar drought index sensitive to global warming: The Standardized Precipitation Evapotranspiration Index. *J. Clim.* **2010**, *23*, 1696–1718. [CrossRef]
21. Kaptue, A.T.; Hanan, N.P.; Prihodko, L.; Ramirez, J.A. Spatial and temporal characteristics of rainfall in Africa: Summary statistics for temporal downscaling. *Water Resour. Res.* **2015**, *51*, 2668–2679. [CrossRef]
22. Li, X.; Zhang, Q.; Ye, X. Dry/Wet Conditions Monitoring Based on TRMM Rainfall Data and Its Reliability Validation over Poyang Lake Basin, China. *Water* **2013**, *5*, 1848–1864. [CrossRef]
23. Liu, J.; Duan, Z.; Jiang, J.; Zhu, A.X. Evaluation of three satellite precipitation products TRMM 3B42, CMORPH, and PERSIANN over a subtropical watershed in China. *Adv. Meteorol.* **2015**, *2015*, 151239. [CrossRef]
24. Naumann, G.; Barbosa, P.; Carrao, H.; Singleton, A.; Vogt, J. Monitoring drought conditions and their uncertainties in Africa using TRMM data. *J. Appl. Meteorol. Climatol.* **2012**, *51*, 1867–1874. [CrossRef]
25. Wardlow, B.; Anderson, M.C.; Verdin, J. *Remote Sensing of Drought: Innovative Monitoring Approaches*; CRC Press: Boca Raton, FL, USA, 2011; p. 484.
26. Cimini, D.; Romano, F.; Ricciardelli, E.; Di Paola, F.; Viggiano, M.; Marzano, F.S.; Colaiuda, V.; Picciotti, E.; Vulpiani, G.; Cuomo, V. Validation of satellite OPEMW precipitation product with ground-based weather radar and rain gauge networks. *Atmos. Meas. Tech.* **2013**, *6*, 3181–3196. [CrossRef]
27. Di Paola, F.; Ricciardelli, E.; Cimini, D.; Romano, F.; Viggiano, M.; Cuomo, V. Analysis of catania flash flood case study by using combined microwave and infrared technique. *J. Hydrometeorol.* **2014**, *15*, 1989–1998. [CrossRef]
28. Price, C.; Yair, Y.; Mugnai, A.; Lagouvardos, K.; Llasat, M.C.; Michaelides, S.; Dayan, U.; Dietrich, S.; Di Paola, F.D.; Galanti, E.; et al. Using Lightning Data to Better Understand and Predict Flash Floods in the Mediterranean. *Surv. Geophys.* **2011**, *32*, 733–751. [CrossRef]
29. Mugnai, A.; Casella, D.; Cattani, E.; Dietrich, S.; Laviola, S.; Levizzani, V.; Panegrossi, G.; Petracca, M.; Sanò, P.; Di Paola, F.; et al. Precipitation products from the hydrology SAF. *Nat. Hazards Earth Syst. Sci.* **2013**, *13*, 1959–1981. [CrossRef]
30. Casella, D.; Dietrich, S.; Di Paola, F.; Formenton, M.; Mugnai, A.; Porcù, F.; Sanò, P. PM-GCD—A combined IR–MW satellite technique for frequent retrieval of heavy precipitation. *Nat. Hazards Earth Syst. Sci.* **2012**, *12*, 231–240. [CrossRef]
31. AghaKouchak, A.; Farahmand, A.; Melton, F.S.; Teixeira, J.; Anderson, M.C.; Wardlow, B.D.; Hain, C.R. Remote sensing of drought: Progress, challenges and opportunities. *Rev. Geophys.* **2015**, *53*, 452–480. [CrossRef]

32. Méndez, M.; Magaña, V. Regional Aspects of Prolonged Meteorological Droughts over Mexico and Central America. *J. Clim.* **2010**, *23*, 1175–1188. [CrossRef]
33. Therrell, M.D.; Stahle, D.W.; Cleaveland, M.K.; Villanueva-Diaz, J. Warm season tree growth and precipitation over Mexico. *J. Geophys. Res.* **2002**, *107*, 4205. [CrossRef]
34. Seager, R.; Ting, M.; Davis, M.; Cane, M.; Naik, N.; Nakamura, J.; Li, C.; Cook, E.; Stahle, D.W. Mexican drought: An observational modeling and tree ring study of variability and climate change. *Atmosphera* **2009**, *22*, 1–31.
35. Seager, R.; Ting, M.; Held, I.; Kushnir, Y.; Lu, J.; Vecchi, G.; Huang, H.-P.; Harnik, N.; Leetmaa, A.; Lau, N.-C.; et al. Model projections of an imminent transition to a more arid climate in southwestern North America. *Science* **2007**, *316*, 1181–1184. [CrossRef] [PubMed]
36. Neri, C.; Magaña, V. Estimation of Vulnerability and Risk to Meteorological Drought in Mexico. *Weather Clim. Soc.* **2016**, *8*, 95–110. [CrossRef]
37. CONAGUA. *Clima en México*; Comisión Nacional del Agua: Mexico City, Mexico, 2015.
38. CONABIO. Comisión Nacional para el Conocimiento y Uso de la Biodiversidad. 1998. Available online: http://www.conabio.gob.mx (accessed on 14 December 2015).
39. Huffman, G.J.; Bolvin, D.T.; Nelkin, E.J.; Wolff, D.B.; Adler, R.F.; Gu, G.; Hong, Y.; Bowman, K.P.; Stocker, E.F. The TRMM multisatellite precipitation analysis (TMPA): Quasiglobal, multiyear, combined-sensor precipitation estimates at fine scales. *J. Hydrometeorol.* **2007**, *8*, 38–55. [CrossRef]
40. Kummerow, C.; Barnes, W.; Kozu, T.; Shiue, J.; Simpson, J. The tropical rainfall measuring mission (TRMM) sensor package. *J. Atmos. Ocean. Technol.* **1998**, *15*, 809–817. [CrossRef]
41. Cashion, J.; Lakshmi, V.; Bosch, D.; Jackson, T.J. Microwave remote sensing of soil moisture: Evaluation of the TRMM microwave imager (TMI) satellite for the Little River Watershed Tifton, Georgia. *J. Hydrol.* **2005**, *307*, 242–253. [CrossRef]
42. Chang, A.T.C.; Chiu, L.S.; Kummerow, C.; Meng, J.; Wilheit, T.T. First results of the TRMM Microwave Imager (TMI) monthly oceanic rain rate: Comparison with SSM/I. *Geophys. Res. Lett.* **1999**, *26*, 2379–2382. [CrossRef]
43. Mugnai, A.; Smith, E.A.; Tripoli, G.J.; Bizzarri, B.; Casella, D.; Dietrich, S.; Di Paola, F.; Panegrossi, G.; Sanò, P. CDRD and PNPR satellite passive microwave precipitation retrieval algorithms: EuroTRMM/EURAINSAT origins and H-SAF operations. *Nat. Hazards Earth Syst. Sci.* **2013**, *13*, 887–912. [CrossRef]
44. Hollinger, J.P.; Peirce, J.L.; Poe, G.A. SSM/I instrument evaluation. *IEEE Transact. Geosci. Remote Sens.* **1990**, *28*, 781–790. [CrossRef]
45. Spencer, R.W.; Goodman, H.M.; Hood, R.E. Precipitation retrieval over land and ocean with the SSM/I: Identification and characteristics of the scattering signal. *J. Atmos. Ocean. Technol.* **1989**, *6*, 254–273. [CrossRef]
46. Kawanishi, T.; Sezai, T.; Ito, Y.; Imaoka, K.; Takeshima, T.; Ishido, Y.; Shibata, A.; Miura, M.; Inahata, H.; Spencer, R.W. The Advanced Microwave Scanning Radiometer for the Earth Observing System (AMSR-E), NASDA's contribution to the EOS for global energy and water cycle studies. *IEEE Trans. Geosci. Remote Sens.* **2003**, *41*, 184–194. [CrossRef]
47. Lobl, E.S.; Aonashi, K.; Murakami, M.; Griffith, B.; Kummerow, C.; Liu, G.; Wilheit, T. Wakasa Bay: An AMSR precipitation validation campaign. *Bull. Am. Meteorol. Soc.* **2007**, *88*, 551–558. [CrossRef]
48. Sanò, P.; Panegrossi, G.; Casella, D.; Di Paola, F.; Milani, L.; Mugnai, A.; Petracca, M.; Dietrich, S. The Passive microwave Neural network Precipitation Retrieval (PNPR) algorithm for AMSU/MHS observations: Description and application to European case studies. *Atmos. Meas. Tech.* **2015**, *8*, 837–857. [CrossRef]
49. Di Paola, F.; Casella, D.; Dietrich, S.; Mugnai, A.; Ricciardelli, E.; Romano, F.; Sanò, P. Combined MW-IR Precipitation Evolving Technique (PET) of convective rain fields. *Nat. Hazards Earth Syst. Sci.* **2012**, *12*, 3557–3570. [CrossRef]
50. Guttman, N.B. Accepting the Standardized Precipitation Index: A calculation algorithm. *J. Am. Water Resour. Assoc.* **1999**, *2*, 311–322. [CrossRef]
51. Wu, H.; Hayes, M.J.; Wilhite, D.A.; Svoboda, M. The effect of the length of record on the standardized precipitation index calculation. *Int. J. Climatol.* **2005**, *25*, 505–520. [CrossRef]
52. Guttman, N.B. Comparing the palmer drought index and the standardized precipitation index. *J. Am. Water Resour. Assoc.* **1998**, *34*, 113–121. [CrossRef]

53. Peterson, T.C.; Hoerling, M.P.; Stott, P.A.; Herring, S. Explaining Extreme Events of 2012 from a Climate Perspective. *Bull. Am. Meteor. Soc.* **2012**, *94*, S1–S74. [CrossRef]
54. Husak, G.J.; Michaelsen, J.; Funk, C. Use of the gamma distribution to represent monthly rainfall in Africa for drought monitoring applications. *Int. J. Climatol.* **2007**, *27*, 935–944. [CrossRef]
55. Peterson, T.C.; Stott, P.A.; Herring, S. Explaining Extreme Events of 2011 from a Climate Perspective. *Bull. Am. Meteorol. Soc.* **2012**, *93*, 1041–1067. [CrossRef]